

PARTICLES AND FIELDS • OPEN ACCESS

Cross section and Higgs mass measurement with Higgsstrahlung at the CEPC^{*}

To cite this article: Zhen-Xing Chen *et al* 2017 *Chinese Phys. C* **41** 023003

View the [article online](#) for updates and enhancements.

You may also like

- [Expected measurement precision of the branching ratio of the Higgs boson decaying to the di-photon at the CEPC](#)
Fangyi Guo, , Yaquan Fang et al.
- [Search for invisible decays of the Higgs boson produced at the CEPC](#)
Yuhang Tan, , Xin Shi et al.
- [Physics cross sections and event generation of \$e^+e^-\$ annihilations at the CEPC](#)
Xin Mo, , Gang Li et al.

Cross section and Higgs mass measurement with Higgsstrahlung at the CEPC^{*}

Zhen-Xing Chen (陈振兴)^{1,2;1)} Ying Yang (杨迎)² Man-Qi Ruan (阮曼奇)^{2;2)}
 Da-Yong Wang (王大勇)^{1;3)} Gang Li (李刚)² Shan Jin (金山)² Yong Ban (班勇)¹⁾

¹ State Key Laboratory of Nuclear Physics and Technology, Peking University, Beijing 100871, China

² Institute of High Energy Physics, Chinese Academy of Sciences, Beijing 100049, China

Abstract: The Circular Electron Positron Collider (CEPC) is a future Higgs factory proposed by the Chinese high energy physics community. It will operate at a center-of-mass energy of 240–250 GeV. The CEPC will accumulate an integrated luminosity of 5 ab^{-1} over ten years of operation, producing one million Higgs bosons via the Higgsstrahlung and vector boson fusion processes. This sample allows a percent or even sub-percent level determination of the Higgs boson couplings. With GEANT4-based full simulation and a dedicated fast simulation tool, we have evaluated the statistical precisions of the Higgsstrahlung cross section σ_{ZH} and the Higgs mass m_{H} measurement at the CEPC in the $Z \rightarrow \mu^+ \mu^-$ channel. The statistical precision of σ_{ZH} (m_{H}) measurement could reach 0.97% (6.9 MeV) in the model-independent analysis which uses only the information from Z boson decays. For the standard model Higgs boson, the m_{H} precision could be improved to 5.4 MeV by including the information from Higgs decays. The impact of the TPC size on these measurements is investigated. In addition, we studied the prospect of measuring the Higgs boson decaying into invisible final states at the CEPC. With the Standard Model ZH production rate, the upper limit of $\mathcal{B}(\text{H} \rightarrow \text{inv.})$ could reach 1.2% at 95% confidence level.

Keywords: CEPC, Higgs mass, cross section

PACS: 13.66Fg, 14.80.Bn, 13.66.Jn **DOI:** 10.1088/1674-1137/41/2/023003

1 Introduction

The Higgs boson has been studied extensively since its discovery [1, 2] at the LHC. The up-to-date results indicate that it is highly Standard Model (SM) like [3–8]. Many new physics models, however, predict the Higgs couplings deviate from the SM at the percent level. Thus, percent or even sub-percent level precision becomes necessary for the future Higgs measurement program. However, this accuracy is difficult to achieve at the LHC [9]. Moreover, as the Higgs boson can only be reconstructed through its decay products at the LHC, it is impossible for the LHC to access the Higgs total width or absolute couplings in a model-independent way.

Compared to a hadron collider, an electron positron collider has significant advantages in precision measurements of the Higgs boson. The beam energy and polarization of the initial states are precisely known and

adjustable. Thus, the Higgs production cross section is available with the recoil technique. In this way, a lepton collider can provide absolute measurements of Higgs couplings [10–12]. Besides, it is free of the QCD backgrounds. Almost every Higgs event can be recorded and reconstructed. Therefore, an electron-positron Higgs factory is an essential step in understanding the nature of the Higgs boson.

The Circular Electron Positron Collider is a Higgs factory proposed by the Chinese high energy physics community [12]. It will operate at a center-of-mass energy of 240–250 GeV with an instantaneous luminosity of $2 \times 10^{34} \text{ cm}^{-2} \text{ s}^{-1}$. With two detectors operating over 10 years, the CEPC will accumulate about one million Higgs events, corresponding to an integrated luminosity of 5 ab^{-1} .

The SM Higgs bosons are produced via the processes of $e^+e^- \rightarrow \text{ZH}$ (Higgsstrahlung), $e^+e^- \rightarrow \nu\bar{\nu}\text{H}$ (WW fu-

Received 21 January 2016, Revised 25 October 2016

^{*} Supported by the Joint Funds of the NSFC (U1232105) and CAS Hundred Talent Program (Y3515540U1)

1) E-mail: zxchen@ihep.ac.cn

2) E-mail: ruanmq@ihep.ac.cn

3) E-mail: dayong.wang@pku.edu.cn



Content from this work may be used under the terms of the Creative Commons Attribution 3.0 licence. Any further distribution of this work must maintain attribution to the author(s) and the title of the work, journal citation and DOI. Article funded by SCOAP³ and published under licence by Chinese Physical Society and the Institute of High Energy Physics of the Chinese Academy of Sciences and the Institute of Modern Physics of the Chinese Academy of Sciences and IOP Publishing Ltd

sion) and $e^+e^- \rightarrow e^+e^-H$ (ZZ fusion) at the CEPC [13–18], as shown in Fig. 1. The corresponding production cross sections for the SM Higgs boson of 125 GeV, as functions of center-of-mass energy, are plotted in Fig. 2. At the center-of-mass energy of 250 GeV, the Higgs bosons are dominantly produced from the ZH process, where the Higgs boson is produced in association with a Z boson.

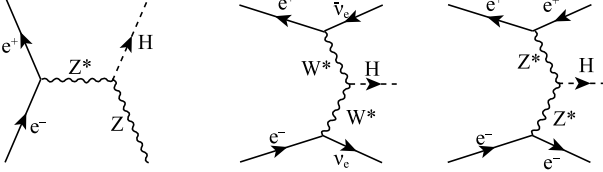


Fig. 1. Feynman diagrams of the Higgs production mechanisms at the CEPC: the Higgsstrahlung, WW fusion, and ZZ fusion processes.

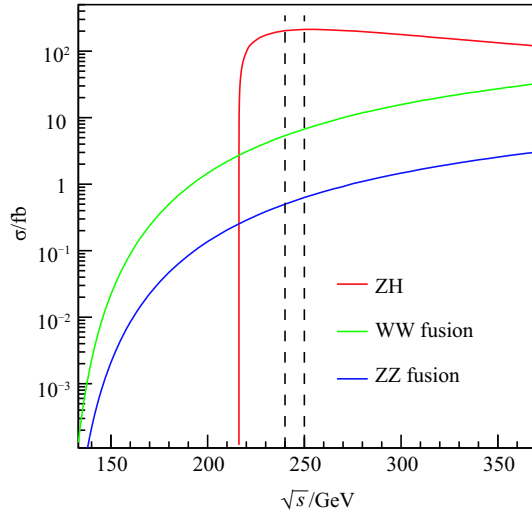


Fig. 2. (color online) Production cross sections of the Higgsstrahlung, WW fusion and ZZ fusion processes as functions of center-of-mass energy. The dashed lines (black) give the possible working energy range of the CEPC.

The branching ratio of the Z boson decaying into a pair of muons is 3.3%. The muons can be easily identified and their momentum can be precisely measured in the detector. By tagging the muon pairs from the associated Z boson decays, the Higgsstrahlung events can be reconstructed with the recoil mass method:

$$M_{\text{recoil}} = \sqrt{s + M_{\mu^+\mu^-}^2 - 2(E_{\mu^+} + E_{\mu^-})\sqrt{s}},$$

where E_{μ^+} and E_{μ^-} are the energies of the two muons, $M_{\mu^+\mu^-}$ is their invariant mass, and s is the square of center-of-mass energy. Therefore, the ZH ($Z \rightarrow \mu^+\mu^-$) events form a peak in the M_{recoil} distribution at the Higgs boson mass.

With the recoil mass method, the ZH events are selected without using the decay information of the Higgs boson. Thus the inclusive ZH cross section σ_{ZH} and the coupling g_{HZZ} can be determined in a model-independent manner. The measured g_{HZZ} , combined with exclusive Higgs boson decay measurements, could be used to determine the Higgs boson width and absolute values of couplings between the Higgs boson and its decay final states [19]. Meanwhile, the Higgs mass m_{H} can be extracted from the M_{recoil} distribution. A good knowledge of the Higgs mass is crucial since m_{H} is the only free parameter in the SM Higgs potential and it determines the Higgs decay branching ratios in the SM. Based on the model-independent analysis, the Higgs decay information can be used to further suppress the backgrounds, leading to a better m_{H} precision.

The recoil mass method allows better exclusive measurement of Higgs decay channels. Many new physics models predict a significant branching ratio of the Higgs boson decaying to invisible products [20–23]. At the LHC, the current upper limit of this branching ratio is about 40% [24, 25], which is much larger than the value predicted in the SM ($\mathcal{B}(\text{H} \rightarrow \text{inv.}) = \mathcal{B}(\text{H} \rightarrow \text{ZZ} \rightarrow \nu\nu\bar{\nu}\bar{\nu}) = 1.06 \times 10^{-3}$). At the CEPC, this measurement can be significantly improved by using the recoil mass method. In this paper, we evaluate the upper limit on the branching ratio of the Higgs decaying to invisible final states.

A series of simulation studies of similar processes have been performed at the International Linear Collider (ILC) [10, 26]. Compared to the ILC, the collision environment of the CEPC is significantly different. The ILC uses polarized beams while the CEPC has no beam polarization. Besides, the beam spot size of the CEPC at the interaction point (IP) is much larger than that of the ILC, leading to a much weaker beamstrahlung effect and a narrower beam energy spread [10, 12, 27]. The details of parameter comparison are listed in Table 1 [27]. Due to the above differences, the cross sections for both signal and backgrounds are different. Therefore, it is necessary to perform a full detector simulation for the CEPC.

Table 1. Comparison of machine and beam parameters between the CEPC and the ILC.

parameters	CEPC	ILC
horizontal beam size at IP	73700 nm	729 nm
vertical beam size at IP	160 nm	7.7 nm
beamstrahlung parameter	4.7×10^{-4}	2.0×10^{-2}
beam energy spread	0.16%	0.24%
integrated luminosity	5 ab^{-1}	2 ab^{-1}

This paper is organized as follows. Section 2 describes the detector model, Monte Carlo (MC) simulation and samples used in the studies. Section 3.1 presents the

measurements of ZH cross section and the Higgs mass in a model-independent manner. The dependencies of measurement precisions on the TPC radii are investigated in Section 3.2, providing a reference for future detector optimization. A model-dependent analysis of the Higgs boson mass is described in Section 3.3, and the measurement of the Higgs decaying to invisible final states is presented in Section 3.4. In Section 4, we discuss the systematic uncertainties and the methodology of systematic control. A conclusion is given in Section 5.

2 Detector and Monte Carlo simulation

The analysis is performed on MC samples simulated on the CEPC conceptual detector, which is based on the International Large Detector (ILD) [28, 29] at the ILC [10]. With respect to the ILD, the CEPC conceptual detector has a L^* (the distance between the interaction point and QD0, the final focusing magnet) of 1.5 m, which is significantly shorter than that of the ILC (4.5 m). The shorter L^* is essential to achieve a high luminosity by reducing the beam nonlinearity in the interaction region. Besides, the CEPC has multiple interaction points, so push-pull operation is not necessary. Therefore, the thickness of the return yoke is reduced by 1 meter at the CEPC conceptual detector.

Apart from the L^* and the return yoke, the CEPC conceptual detector follows the same design as the ILD. Installed in a solenoidal magnet of strength 3.5 T, the CEPC conceptual detector consists of a vertex detector, a tracking system and a calorimetry system. The silicon pixel vertex detector (VTX) consists of three cylindrical and concentric double-layers, with an innermost radius of 16 mm [28, 29]. The tracking system is composed of a time projection chamber (TPC) as the main tracker and the silicon tracking devices, including a silicon inner tracker (SIT), forward tracking disks (FTDs), a silicon external tracker (SET) and end-cap tracking disks. The VTX and SIT are expected to provide a spatial resolution of better than 3 μm near the interaction point, which is crucial for the vertex reconstruction and the jet flavor tagging. The outermost FTD disk is positioned at $z = 1057.5$ mm to the IP. With an inner radius of 92.7 mm and an outer radius of 309 mm, it improves the geometric acceptance of the tracking system to $|\cos\theta| < 0.995$. The TPC has nearly 200 three-dimensional (r , ϕ and z) spacepoints, with inner and outer radii of 0.325 m and 1.8 m respectively, and a half-length of 2.35 m. It provides an expected spatial resolution of better than 100 μm in the $r\phi$ plane. The SET provides a precise position measurement outside the TPC. Such a tracking system is expected to achieve a precise determination of the charged particle momenta with a resolution of $\sigma_{1/p_T} = 2 \times 10^{-5} \oplus 10^{-3}/(p_T \cdot \sin\theta)$, where p_T is the trans-

verse momentum and θ is the polar angle. The calorimetry system is composed of a high granularity electromagnetic calorimeter and a high granularity hadron calorimeter, allowing excellent separations of showers of different particles. It is expected to provide a jet energy resolution of 3%–4% and enable the PID efficiency to be over 99.5% for muons with momentum larger than 10 GeV. More information about the CEPC conceptual detector can be found in Ref. [12].

A set of event samples at a center-of-mass energy of 250 GeV, corresponding to an integrated luminosity of 5 ab^{-1} , has been generated with Whizard 1.95 [30, 31]. It consists of the SM Higgs signal with $m_H = 125$ GeV and the major SM backgrounds, including the $\gamma\gamma$ process (photon-induced background $e^+e^- \rightarrow e^+e^-\gamma\gamma \rightarrow e^+e^-1^+1^-$, where the photons are generated according to the Weizsäcker-Williams approximation [32–34]), 2-fermion processes ($e^+e^- \rightarrow f\bar{f}$, where $f\bar{f}$ refers to all lepton and quark pairs) and 4-fermion processes, categorized as ZZ, WW, ZZ or WW, single Z (e^+e^-Z) and single W ($e^+\nu_e W$ or $e^-\bar{\nu}_e W$). If the final states could be produced through both WW and ZZ intermediate states, such as $e^+e^-\nu_e\bar{\nu}_e$, this process is classified as “ZZ or WW” and their interference is included. The initial state radiation (ISR) is also taken into account in the sample generation. More details about the CEPC samples can be found in reference [35].

The Higgs signal samples are fully simulated with Mokka [36] and reconstructed with ArborPFA [37]. A beam energy spread of 0.16% has been included in this analysis. In order to save computing power, a fast simulation framework has been developed to process the backgrounds. In the fast simulation, the detector responses are obtained by a series of full simulations for single particle events. Then the responses, including momentum resolution and detection efficiency, have been parameterized as functions of energy and polar angle for different types of particles. The four-momenta of the visible final state particles are smeared according to the parameterized resolutions and they are randomly accepted based on the corresponding detection efficiencies.

3 Analyses

The expected number of ZH events N_{ZH} can be expressed as

$$N_{\text{ZH}} = \sigma_{\text{ZH}} \cdot \mathcal{L} \cdot \sum_X \epsilon(\text{H} \rightarrow X) \cdot \mathcal{B}(\text{H} \rightarrow X), \quad (1)$$

where \mathcal{L} is the integrated luminosity, $\mathcal{B}(\text{H} \rightarrow X)$ is the branching ratio of an exclusive Higgs decay mode, and $\epsilon(\text{H} \rightarrow X)$ is the corresponding selection efficiency. In the model-independent analysis using only information in the Z boson decays, the efficiencies are expected to be

uniform for each Higgs decay mode, and we can write

$$N_{ZH} = \sigma_{ZH} \cdot \mathcal{L} \cdot \epsilon \cdot \sum_X \mathcal{B}(H \rightarrow X) = \sigma_{ZH} \cdot \mathcal{L} \cdot \epsilon. \quad (2)$$

Thus σ_{ZH} can be determined in a model-independent manner. The Higgs decay information can be used to further suppress the SM backgrounds and improve the precision of the mass measurement. In this case, the selection efficiency $\epsilon(H \rightarrow X)$ depends on the Higgs decay mode.

3.1 Model-independent analysis of σ_{ZH} and m_H measurement

In the model-independent analysis, the event selection is composed of a pre-selection and a multivariate analysis (MVA). In the pre-selection, a pair of oppositely charged muons is required. The pair with the minimum $|M_{\mu^+\mu^-} - M_Z|$ is selected in case of multi-combinations, where M_Z is 91.2 GeV [38]. The invariant mass of $\mu^+\mu^-$ is required to satisfy $80 \text{ GeV} < M_{\mu^+\mu^-} < 100 \text{ GeV}$. In order to suppress 2-fermion backgrounds, the transverse momentum of the muon pair, $p_{T\mu^+\mu^-}$, is required to be larger than 20 GeV and the difference of the azimuth angles of the two muons should be less than 175° . The Toolkit for Multivariate Analysis (TMVA) [39] is used for further background rejection. In this paper, the method of gradient Boosted Decision Trees (BDT) is adopted and the selected variables for TMVA input are $M_{\mu^+\mu^-}$, $p_{T\mu^+\mu^-}$, the polar angle of the Z candidate, and the acollinearity of the muon pair, which is defined as

$$\text{acol} = \cos^{-1} \frac{\mathbf{p}_{\mu^+} \cdot \mathbf{p}_{\mu^-}}{|\mathbf{p}_{\mu^+}| \cdot |\mathbf{p}_{\mu^-}|}, \quad (3)$$

where \mathbf{p}_{μ^\pm} is the momentum vector of μ^\pm . After the pre-selection, half of the remaining backgrounds are selected for training, together with another copy of the signal

sample of 5 ab^{-1} . The BDT response is calculated using weights obtained from the training samples and applied to the whole data set, shown in Fig. 3. With the requirement of $\text{BDT} > -0.05$, the signal/background ratio is improved from 12.3% to 31.1%.

The BDT selection is optimized to the σ_{ZH} measurement. The cut flow is summarized in Table 2 and the signal selection efficiency is 62.8%. After the selection, the leading backgrounds are from ZZ (18.8% of the remaining background), $\gamma\gamma$ (21.8%) and 2-fermion (32.8%) processes. The selected muons may also come from the ZH events with the Z boson not decaying to $\mu^+\mu^-$. About 200 events of this type survive after the event selection and they are flatly distributed in the signal region. They are neglected due to their small contribution ($\sim 0.29\%$) to the total background.

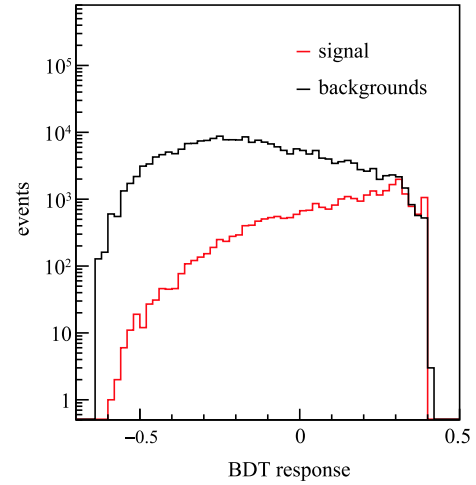


Fig. 3. (color online) The BDT response for the signal and background samples. The red solid line is signal and the black dashed line is background. The number of background events is normalized to that of signal.

Table 2. Efficiencies of signal and background in the model-independent analysis

	Z($\mu^+\mu^-$)H	ZZ	WW	ZZ or WW	single Z	Z(2f)	$\gamma\gamma$
total generated	35247	5347053	44180832	17801222	7809747	418595861	161925000
$N_{\mu^+} \geq 1, N_{\mu^-} \geq 1$	95.7%	11.95%	0.65%	3.92%	9.75%	1.64%	17.31%
$120 \text{ GeV} < M_{\text{recoil}} < 150 \text{ GeV}$	93.2%	1.71%	0.23%	0.70%	1.93%	0.17%	3.06%
$80 \text{ GeV} < M_{\mu^+\mu^-} < 100 \text{ GeV}$	85.5%	0.68%	0.06%	0.22%	0.22%	0.10%	0.11%
$p_{T\mu^+\mu^-} > 20 \text{ GeV}$	80.2%	0.57%	0.06%	0.17%	0.16%	0.02%	0.04%
$\Delta\phi < 175^\circ$	77.8%	0.51%	0.05%	0.17%	0.15%	0.01%	0.04%
BDT cut	63.0%	0.25%	0.01%	0.05%	0.06%	0.01%	0.01%
fit window	62.8%	0.25%	0.01%	0.05%	0.05%	0.01%	0.01%

The final recoil mass spectrum of $\mu^+\mu^-$ is shown in Fig. 4. An unbinned maximum likelihood fit to the M_{recoil} distribution is performed in the region of 120 GeV to 140 GeV to determine the signal yield as well as the

value of the Higgs mass. The background is represented by a third order Chebychev polynomial function, whose parameters are fixed to the values extracted from the background samples. The Higgs signal shape is described

by a Crystal Ball function. Based on the fit results, σ_{ZH} is estimated to a relative precision of 0.97% and m_H to a precision of 6.9 MeV.

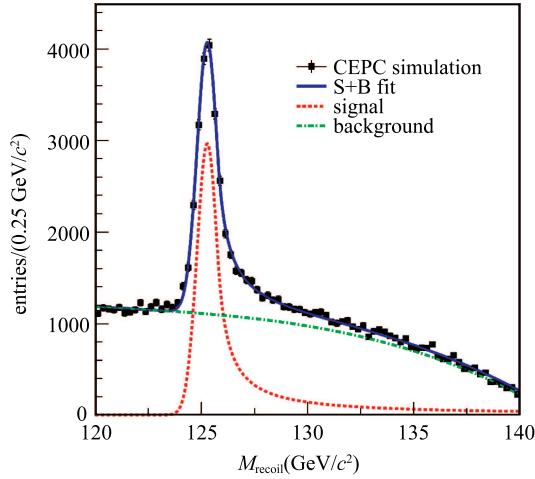


Fig. 4. (color online) The recoil mass spectrum of $\mu^+\mu^-$ in the model-independent analysis. The dots with error bars represent the CEPC simulation. The solid (blue) line indicates the fit. The dashed (red) and the long-dashed (green) line show the signal and the background contributions in the fit, respectively.

The uniformity of event selection efficiency with different Higgs decay modes is studied. A SM ZH ($Z \rightarrow \mu^+\mu^-$) sample corresponding to 500 ab^{-1} has been simulated, where the Higgs boson decays inclusively. Figure 5 shows the efficiencies and no significant bias to any specific Higgs decay mode is observed. In order to evaluate

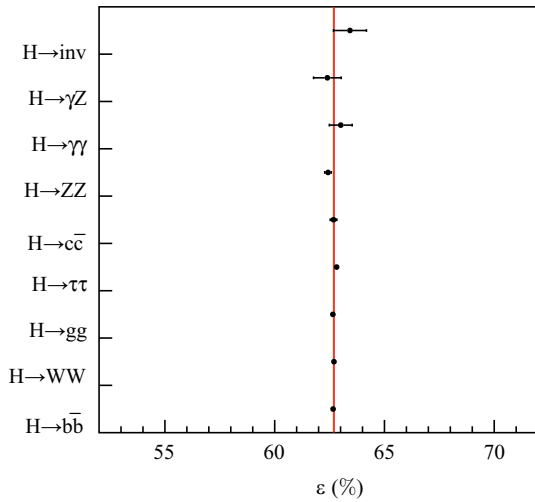


Fig. 5. (color online) The efficiencies for main decay modes of the Higgs boson in model-independent analysis. The dots with error bars are efficiencies from exclusive channels. The solid line (red) is the event selection efficiency of model-independent analysis.

the impact of the sensitivities to the various Higgs decay modes, the SM ZH cross section is kept unchanged and a specific SM Higgs decay branching ratio is enlarged by 5% each time ($\mathcal{B}(H \rightarrow X) \rightarrow \mathcal{B}(H \rightarrow X) + 5\%$). All branching ratios are then scaled to keep the total event rate and the resultant differences in the σ_{ZH} measurement are summarized in Table 3. The largest bias in the σ_{ZH} is less than 10^{-3} , which is much smaller than the statistical uncertainty 0.97%. It is therefore reasonable to conclude the recoil mass method gives a model-independent measurement.

Table 3. Estimation of biases of σ_{ZH} caused by potential variances of the Higgs decay branching ratios.

decay mode	bias ($\times 10^{-4}$)
$H \rightarrow b\bar{b}$	-0.10
$H \rightarrow WW$	+0.20
$H \rightarrow gg$	-0.18
$H \rightarrow \tau\tau$	+1.11
$H \rightarrow c\bar{c}$	+0.05
$H \rightarrow ZZ$	-1.85
$H \rightarrow \gamma\gamma$	+2.56
$H \rightarrow \gamma Z$	-2.08
$H \rightarrow \text{inv.}$	+5.75

3.2 Dependency of σ_{ZH} and m_H measurement accuracies on the TPC radius

From the detector point of view, the precisions of σ_{ZH} and m_H are mainly determined by the detector solid angle acceptance and the muon identification efficiency. Besides, the m_H precision also relies on the muon momentum resolution. The momentum resolution scales approximately with the inverse of BL^2 , where B and L represent the magnetic field strength and the detector radius respectively. The tracking system of the CEPC conceptual detector is composed of a silicon tracking system and a main TPC tracker. A larger TPC radius, corresponding to a larger lever arm, will give a better momentum resolution but is more expensive to construct. The performances at different TPC radii are studied using the fast simulation tool. In the model-independent analysis, the expected accuracies of σ_{ZH} and m_H are recorded, as shown in Fig. 6. If the TPC radius is reduced by 25%, the precisions of σ_{ZH} and m_H are worsened by 2% and 20%, respectively. These expected accuracies are then parameterized as functions of the TPC radius. For the σ_{ZH} measurement, it is expressed as

$$\frac{\delta\sigma_{ZH}}{\sigma_{ZH}} = 0.52 \times (1 + e^{-0.09 \cdot R_{\text{TPC}}}), \quad (4)$$

where $\frac{\delta\sigma_{ZH}}{\sigma_{ZH}}$ (%) is the relative precision of cross section measurement and R_{TPC} (m) is the TPC radius. Similarly, the accuracies of Higgs mass δm_H at different TPC radii are obtained. Its dependence on the TPC radius can be expressed as

$$\delta m_H = 5.85 \times (1 + 5.19 \times e^{-1.81 \cdot R_{\text{TPC}}}) \text{ MeV}. \quad (5)$$

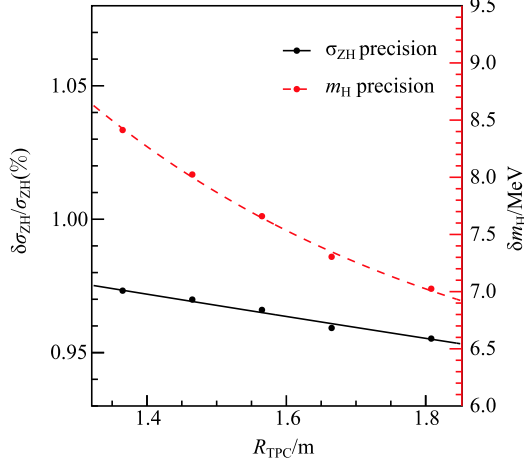


Fig. 6. The precisions of σ_{ZH} and m_H measurements versus different TPC radii. The solid line represents the precision of σ_{ZH} , and the dashed line is for m_H .

3.3 Model-dependent analysis on m_H measurement

Assuming SM Higgs decays, the background can be further suppressed by using the Higgs decay information, leading to a better Higgs mass measurement. On top of the pre-selection criteria used in the model-independent analysis, we request that there are more than four charged tracks reconstructed. In the MVA stage, the energy of all reconstructed final states, E_{vis} , is also taken as an input variable except those in the MVA of model-independent analysis. After the final selection, the recoil mass spectrum is shown in Fig. 7 and an efficiency of 66.1% is obtained. The resultant precision of m_H is improved to 5.4 MeV.

3.4 Measurement of the Higgs boson invisible decay mode

The invisible decay mode of the Higgs boson is a well motivated signature of physics beyond the SM [20–23]. At the CEPC, the invisible Higgs boson decay branching ratio can be determined precisely using the recoil mass method. Assuming the Higgs boson has a SM coupling to the Z boson and non-vanishing couplings to the beyond-SM invisible particles, the measurement potential of the Higgs boson decaying to invisible final states at the CEPC is investigated at different values of $\mathcal{B}(H \rightarrow \text{inv.})$.

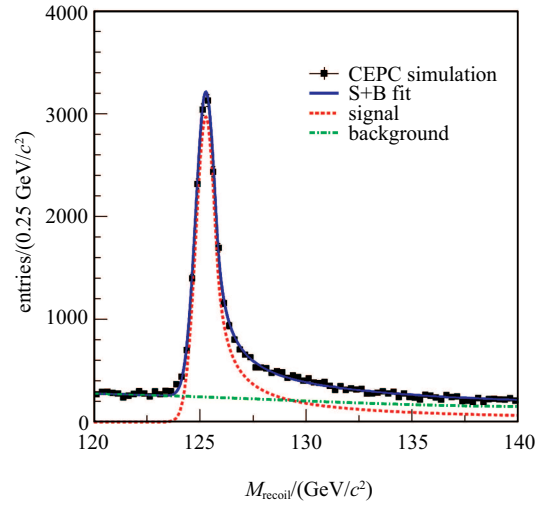


Fig. 7. (color online) The recoil mass spectrum of $\mu^+\mu^-$ in the model-dependent analysis. The dots with error bars represent the CEPC simulation. The solid (blue) line indicates the fit. The dashed (red) and the long-dashed (green) line are the signal and the background, respectively.

The signal candidates are identified using the same pre-selection as that in the model-independent analysis. In addition, we require that there is no extra visible energy except that of the muon pair decayed from the Z boson and that E_{vis} must be within 105 GeV and 125 GeV. Figure 8 shows the $\mu^+\mu^-$ recoil mass spectrum of the candidates with $\mathcal{B}(H \rightarrow \text{inv.}) = 50\%$. In this scenario, the final signal event selection efficiency is 63.9% and the relative precision of the cross section of Higgs decaying to invisible final states $\delta\sigma_{ZH,H \rightarrow \text{inv.}}/\sigma_{ZH,H \rightarrow \text{inv.}}$ reaches 1.16%.

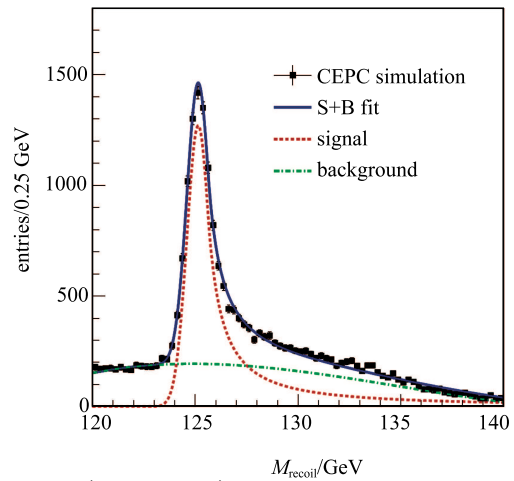


Fig. 8. (color online) The recoil mass spectrum of $\mu^+\mu^-$ in the measurement of the invisible decay mode of the Higgs boson with $\mathcal{B}(H \rightarrow \text{inv.}) = 50\%$. The dots with error bars represent the CEPC simulation. The solid (blue) line indicates the fit. The dashed (red) and the long-dashed (green) line are the signal and the background, respectively.

Based on different assumptions of $\mathcal{B}(H \rightarrow \text{inv.})$, the relative precisions of $\delta\sigma_{ZH,H \rightarrow \text{inv.}}/\sigma_{ZH,H \rightarrow \text{inv.}}$ are given in Fig. 9. The upper limit of $\mathcal{B}(H \rightarrow \text{inv.})$ at 95% confidence level is estimated to be 1.2×10^{-2} by using the likelihood ratio test method [40].

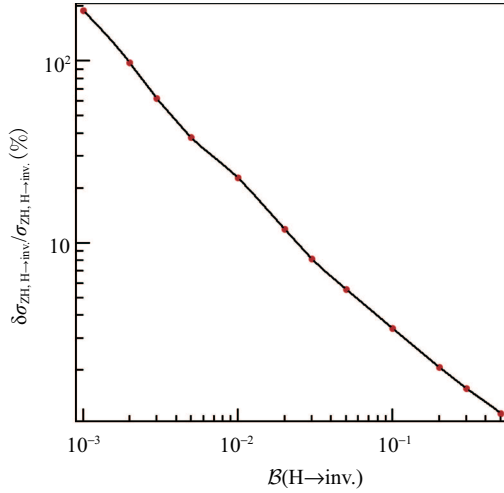


Fig. 9. The precision of the cross section of Higgs decaying to invisible final states $\delta\sigma_{ZH,H \rightarrow \text{inv.}}/\sigma_{ZH,H \rightarrow \text{inv.}}$ versus $\mathcal{B}(H \rightarrow \text{inv.})$.

4 Discussion of systematic uncertainties

A complete investigation of potential systematic uncertainties is beyond the scope of this paper. Here we present several sources of systematic uncertainties and the strategies to deal with them.

The common uncertainties on σ_{ZH} and m_H measurements include differences between the data and the MC simulation for the tracking efficiency and PID, which can be investigated and corrected using a high purity control sample of about 20 M $Z\gamma$ (ISR return) events.

In the measurement of cross sections, the important uncertainties are from ISR correction factor ($1 + \delta$, defined as the ratio of observed cross section over the Born cross section), luminosity measurement, the branching fraction of intermediate state decay ($Z \rightarrow \mu^+\mu^-$), as well as fitting procedure.

The uncertainty of $1 + \delta$ depends on the precisions of both the experimental line shape measurement on the Born σ_{ZH} below 250 GeV and the theoretical radiator function. We expect the latter will be calculated to a precision that is negligible comparing to the statistical uncertainty by the time of CEPC data taking. The former is estimated with Born cross sections at six center-of-mass energies equally distributed from the threshold to 250 GeV. The luminosity is set at 50 fb^{-1} for each energy point below 250 GeV and the cross sections are generated according to the formula in Ref. [35] with statistical uncertainties. The generated cross sections are

fitted with the same formula, but the coupling is free and the Higgs mass is floating within one standard deviation, based on the PDG [38]. Then the resultant line shape is used to calculate the $1 + \delta$. We repeat the generation, fitting, and calculation procedure 1000 times, and the spread of $1 + \delta$ is determined to be 0.1% and taken as the systematic uncertainty of the correction factor.

The integrated luminosity could be measured using small angle radiative Bhabha scattering and the expected precision is better than 10^{-3} . The current uncertainty in the $\mathcal{B}(Z \rightarrow \mu^+\mu^-)$ is 0.2% [38], which will be further improved by the Z boson samples at the CEPC. The uncertainty of fitting procedure could be estimated by changing the background shape and fitting range, and the difference in the measured σ_{ZH} is taken as the systematic uncertainty.

In the Higgs mass measurement, the dominant uncertainty may be from beam energy measurement. In order to control this uncertainty to MeV level, new technology needs to be developed to improve the precision of beam energy measurement. Another potential uncertainty is the mass shift between the measured Higgs mass and the truth value. In order to control the shift, the dependence of mass shift on the Higgs mass input is investigated around 125 GeV. Then it is extracted as a third order Chebychev polynomial function. The measured Higgs mass is corrected by the fit function. The combined uncertainty of fit function and the remaining shift, 1.5 MeV, is taken as the systematic uncertainty.

Consistency between the fast and full simulation is checked using the ZZ events with at least one pair of muons found. The invariant mass of $\mu^+\mu^-$ is shown in Fig. 10. In the region concerned, between 80 GeV and 100 GeV, the statistics of the full-simulated ZZ sample are 2.32% lower than those of the fast-simulated. If the remaining background is reduced by 2% after the final

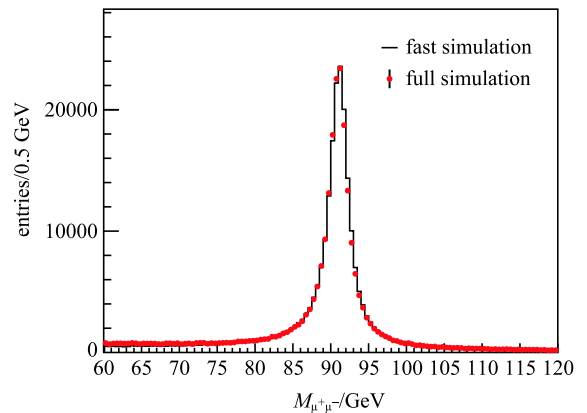


Fig. 10. (color online) The invariant mass spectrum of $\mu^+\mu^-$ from the samples of ZZ background. The red dots with error bars are from full simulation while the black histogram is from fast simulation.

event selection, the precision of σ_{ZH} varies from 0.974% to 0.971% and the m_H precision varies from 6.91 MeV to 6.87 MeV. Therefore, this effect can be safely ignored in this analysis.

From the above discussion, the systematic uncertainty should be under control while the statistical uncertainty will be dominant at the CEPC.

5 Summary

The CEPC is expected to play a crucial role in understanding the nature of the Higgs boson. In this paper, the statistical precisions of Higgs production cross section σ_{ZH} and mass m_H measurements at the CEPC are investigated with full simulated Higgsstrahlung signal of 5 ab^{-1} integrated luminosity at the center-of-mass energy of 250 GeV. Using the recoil mass method, the statistical precision of σ_{ZH} could reach 0.97%, corresponding to a 0.49% accuracy of g_{HZZ} . The expected statistical accuracy of m_H is 6.9 MeV while it is improved to 5.4 MeV with inclusion of the Higgs decay information. The dependence of these results on TPC radius is investigated and parameterized. Reducing the TPC radius by 25%, the statistical precisions of σ_{ZH} and m_H worsen to 0.98% and 8.4 MeV, respectively. In addition, we explored the

potential of the invisible decay mode of the Higgs boson at the CEPC. The upper limit of $\mathcal{B}(H \rightarrow \text{inv.})$ at the 95% confidence level could reach 1.2×10^{-2} . All above results are incorporated into the CEPC-SPPC Preliminary Conceptual Design Report [12].

The same measurement has been studied at the ILC in the $Z \rightarrow e^+e^-$ and $Z \rightarrow \mu^+\mu^-$ channels with an integrated luminosity of 2 ab^{-1} and polarized beams of $P(e^-, e^+) = (-0.8, 0.3)$ [10, 26]. The g_{HZZ} precision could reach 0.4% while the upper limit of $\mathcal{B}(H \rightarrow \text{inv.})$ is 1.7×10^{-2} . For the m_H measurement, the current m_H precision is 0.24 GeV achieved at the LHC [8] and it will be improved to 50 MeV at the HL-LHC [9]. At the ILC, the statistical precision of m_H could reach 14 MeV [10, 26]. Compared with these facilities, the improvement at the CEPC is due to weaker beamstrahlung and higher statistics.

The authors would like to thank the ILD Concept Group for providing a reference of detector and software for the CEPC study. We thank professor Yuan-Ning Gao for fruitful discussion on the analysis technique. We are grateful to Dr. Xin Mo and Yu-Qian Wei for providing high statistical MC samples. We appreciate Dr. Bin-Song Ma on the development of reconstruction algorithm.

References

- 1 G. Aad et al (The ATLAS Collaboration), Phys. Lett. B, **716**: 1 (2012)
- 2 S. Chatrchyan et al (The CMS Collaboration), Phys. Lett. B, **716**: 30 (2012)
- 3 S. Chatrchyan et al (The CMS Collaboration), JHEP, **06**: 081 (2013)
- 4 G. Aad et al (The ATLAS Collaboration), Phys. Lett. B, **726**: 88 (2013)
- 5 G. Aad et al (The ATLAS Collaboration), Phys. Lett. B, **726**: 120 (2013)
- 6 V. Khachatryan et al (The CMS Collaboration), Eur. Phys. J. C, **75**: 212 (2015)
- 7 V. Khachatryan et al (The CMS Collaboration), Phys. Rev. D, **92**: 012004 (2015)
- 8 G. Aad et al (The ATLAS Collaboration and CMS Collaboration), Phys. Rev. Lett., **114**: 191803 (2015)
- 9 S. Dawson, A. Gritsan, H. Logan et al, arXiv:1310.8361
- 10 H. Baer, T. Barklow, K. Fujii et al, arXiv:1306.6352
- 11 K. Eujii et al (LCC Physics Working Group), arXiv:1506.05992
- 12 M. Ahmad et al (The CEPC-SPPC Study Group), CEPC-SppC Preliminary Conceptual Design Report: Physics and Detector, http://cepc.ihep.ac.cn/preCDR/main_preCDR.pdf, retrieved 4th May 2015
- 13 J. Ellis, M.K. Gaillard, and D.V. Nanopoulos, Nucl. Phys. B, **106**: 292 (1976)
- 14 B.L. Ioffe and V.A. Khoze, Sov. J. Part. Nucl., **9**: 50 (1978)
- 15 B.W. Lee, C. Quigg and H.B. Thacker, Phys. Rev. D, **16**: 1519 (1977)
- 16 J.D. Bjorken, Weak-interaction Theory and Neutral Currents, in proceedings of the 1976 SLAC Summer Institute on Particle Physics
- 17 M. Carena, P. Zerwas, E. Accomando et al, arXiv:hep-ph/9602250
- 18 P.M. Zerwas, The Physics Potential, in the Workshop on e^+e^- Collisions at 500 GeV
- 19 C. Durig, K. Fujii, Jenny List et al, arXiv: 1403.7734
- 20 Shouhua Zhu, Chin. Phys. Lett., **24**: 381 (2007)
- 21 G. Belanger, F. Boudjema, A. Cottrant et al, Phys. Lett. B, **519**: 93 (2001)
- 22 G.F. Giudice, R. Rattazzi, J.D. Wells, Nucl. Phys. B, **595**: 250 (2001)
- 23 M. Battaglia, D. Dominici, J.F. Gunion et al, arXiv: hep-ph/0402062
- 24 S. Chatrchyan et al (The CMS Collaboration), Eur. Phys. J. C, **74**: 2980 (2014)
- 25 G. Aad et al (The ATLAS Collaboration), Phys. Rev. Lett., **112**: 201802 (2014)
- 26 J. Yan, S. Watanuki, K. Fujii et al, arXiv:1604.07524
- 27 Q. Xiu, H. Zhu and X. Lou, arXiv:1505.01270
- 28 The ILD concept group, arXiv:1006.3396
- 29 T. Behnke, J. Brau, P. Burrows et al, arXiv: 1306.6329
- 30 W. Kilian, T. Ohl and J. Reuter, Eur. Phys. J. C, **71**: 1742 (2011)
- 31 M. Moretti, T. Ohl and J. Reuter, arXiv: hep-ph/0102195
- 32 C. F. von Weizsäcker, Z. Phys., **88**: 612 (1934)
- 33 E. J. Williams, Phys. Rev., **45**: 729 (1934)
- 34 V. M. Budnev, I. F. Ginzburg, G. V. Meledin and V. G. Serbo, Phys. Rept. **15**: 181 (1974)
- 35 Xin Mo, Gang Li, Manqi Ruan et al, Chin. Phys. C, **40**: 033001 (2016)
- 36 P. Mora de Freitas and H. Videau, Detector simulation with Mokka/Geant4: present and future, in the International Workshop on Linear Colliders (LCWS 2002)
- 37 Manqi Ruan, arXiv: 1403.4784
- 38 K.A. Olive et al., Chin. Phys. C, **38**: 090001 (2014)
- 39 P. Speckmayer, A. Hocker, J. Stelzer et al, J. Phys. Conf. Ser., **219**: 032057 (2010)
- 40 G. Cowan, K. Cranmer, E. Gross et al, Eur. Phys. J. C, **71**: 1554 (2011)